

MODAL DECOMPOSITION OF NON-LINEAR INTERACTIONS IN WALL TURBULENCE

Ugur Karban

Department of Aerospace Engineering
Middle East Technical University
06800 Ankara Turkey
ukarban@metu.edu.tr

Eduardo Martini

Département Fluides, Thermique, Combustion
Institut Pprime, CNRS-University of Poitiers-ENSMA
86073 Poitiers France
eduardo.martini@univ-poitiers.fr

André V. G. Cavalieri

Instituto Tecnológico de Aeronáutica
São José dos Campos/SP, Brazil
andre@ita.br

Peter Jordan

Département Fluides, Thermique, Combustion
Institut Pprime, CNRS-University of Poitiers-ENSMA
86073 Poitiers France
peter.jordan@univ-poitiers.fr

ABSTRACT

Coherent structures are found in many different turbulent flows, and they are known to drive self-sustaining processes in minimal-unit turbulence. Identifying the triadic interactions between coherent structures can provide insights beyond what is possible in the framework of linearised models. There are infinite possible interactions that may generate a given structure, and thus a method to systematically study those, ranking them in terms of their contribution, is of interest. We here use the resolvent-based extended spectral proper orthogonal decomposition (RESPOD) approach (Karban, U. *et al.* 2022 Self-similar mechanisms in wall turbulence studied using resolvent analysis. *Journal of Fluid Mechanics* 969, A36) to identify the relevant triadic interactions for a minimal Couette flow at $Re_\tau = 34$, studying the interactions that give rise to wall-attached structures, obtained by measuring the wall-shear. Our analysis reveals that there are six triadic interactions that dominate the most-energetic wall-attached structure.

1 INTRODUCTION

We investigate dominant nonlinear mechanisms in wall-bounded turbulence. The complexity of all possible triadic interactions in a turbulent flow can be reduced by focusing on a certain quantity and eliminating all the non-relevant interactions. We use the resolvent-based extended spectral proper orthogonal decomposition (RESPOD) (Karban *et al.*, 2022) for this purpose. This should aid to design reduced-order models appropriate for the description of a given observable in a turbulent flow.

We use the resolvent framework (McKeon & Sharma, 2010), where the Navier-Stokes operator linearized around the mean can be used to link the triadic interactions and a flow quantity of interest, which appear, respectively, as forcing and response. Such a linear relation allows us to understand the role of various interactions that appear in *interaction maps* that measure the dominance of a given interaction with respect to a given observable.

The method is implemented using a direct numerical simulation (DNS) of minimal Couette flow with $Re_\tau \approx 34$, where

the spanwise wall shear is considered as the target observable. In similar minimal channel configurations, Bae *et al.* (2021) investigated the triadic interactions contributing to the $(\alpha, \beta) = (0, 2\pi/L_z)$ mode, where α and β are streamwise and spanwise wavenumbers, respectively, and L_z is the domain size in z -direction. We investigate here the triadic interactions systematically extracted using RESPOD for the same mode.

The remainder of the paper is structured as follows: the mathematical framework to extract triadic interactions associated with a measured quantity is explained in §2. The details about the DNS database of the minimal Couette flow are provided in §3. The results about identifying the relevant triadic interactions and the energy transfer via these interactions in the minimal Couette flow are discussed in §4. Finally, some concluding remarks are provided in §5.

2 EXTRACTING NONLINEAR INTERACTIONS USING RESPOD

We consider the incompressible Navier-Stokes (N-S) equations as,

$$\mathbf{M}\partial_t\mathbf{q}(\mathbf{x},t) = \mathcal{N}(\mathbf{q}(\mathbf{x},t)), \quad (1)$$

where $\mathbf{q} = [uvw p]^\top$ is the state vector, \mathcal{N} denotes the nonlinear N-S operator for incompressible flows and the matrix \mathbf{M} is zero for the continuity equation and identity matrix for the rest. Discretisation in space and linearisation around the mean, $\bar{\mathbf{q}}(\mathbf{x})$, yields

$$\mathbf{M}\partial_t\mathbf{q}'(\mathbf{x},t) - \mathbf{A}(\mathbf{x})\mathbf{q}'(\mathbf{x},t) = \mathbf{B}\mathbf{f}(\mathbf{x},t), \quad (2)$$

where $\mathbf{A}(\mathbf{x}) = \partial_q \mathcal{N}|_{\bar{\mathbf{q}}}$ is the linear operator obtained from the Jacobian of \mathcal{N} and $\mathbf{f}(\mathbf{x},t)$ denotes all the remaining nonlinear terms, interpreted as a forcing term in the above equation with $\mathbf{B} = \mathbf{M}$ for this particular case. Without loss of generality, we focus on parallel flow, i.e., a flow that is homogeneous in two

directions, for instance, in x and z , with the mean flow varying only in y . We can modify (2) to cast it in the resolvent form by applying Fourier transforms in all homogeneous dimensions and rearranging as,

$$\hat{\mathbf{q}}(\tilde{\alpha}, y, \tilde{\beta}, \tilde{\omega}) = \mathbf{R}(\tilde{\alpha}, y, \tilde{\beta}, \tilde{\omega}) \hat{\mathbf{f}}(\tilde{\alpha}, y, \tilde{\beta}, \tilde{\omega}), \quad (3)$$

where $\tilde{\alpha}$ and $\tilde{\beta}$ are the streamwise and spanwise wavenumbers, respectively, and $\tilde{\omega}$ is the angular frequency, the hat indicates a Fourier transformed quantity and $\mathbf{R}(\tilde{\alpha}, y, \tilde{\beta}, \tilde{\omega}) = (-i\tilde{\omega}\mathbf{M} - \mathbf{A}(\tilde{\alpha}, y, \tilde{\beta}))^{-1}\mathbf{B}$ is the resolvent operator. For brevity, we drop the notation showing dependence on wavenumber and frequency in what follows.

For the incompressible N-S equations, the forcing term in (2) is given as $\mathbf{f} = \mathbf{u}' \cdot \nabla \mathbf{u}' - \overline{\mathbf{u}' \cdot \nabla \mathbf{u}'}$. The forcing in the wavenumber-frequency space, $\hat{\mathbf{f}}_{\mathbf{k}}$, is then obtained via a convolution,

$$\hat{\mathbf{f}}_{\mathbf{k}} = \sum_{\mathbf{i}} \hat{\mathbf{u}}_{\mathbf{i}} \cdot \nabla \hat{\mathbf{u}}_{\mathbf{k}-\mathbf{i}}, \quad (4)$$

where $\mathbf{i} = (\alpha_i, \beta_i, \omega_i)$, and $\mathbf{k} = (\alpha_k, \beta_k, \omega_k)$ denote wavenumber-frequency combinations and summation over \mathbf{i} implies nested summation over α_i , β_i and ω_i . Note that (4) is valid assuming that the target triplet \mathbf{k} contains at least one non-zero element.

The RESPOD method, adapted from extended proper orthogonal decomposition (Borée, 2003; Hoarau *et al.*, 2006), finds, for a given ‘observed’ SPOD mode of state (response), all correlated parts in a ‘target’ event. Here we choose the target event to be the non linear interactions, which give rise to the forcing terms in the resolvent framework, as in Towne *et al.* (2015) and Karban *et al.* (2022).

The SPOD mode of a measured quantity, $\hat{\mathbf{y}}_{\mathbf{k}}$, can be estimated using the ensemble matrix of realisations, through the eigendecomposition,

$$\hat{\mathbf{Y}}_{\mathbf{k}}^H \mathbf{W} \hat{\mathbf{Y}}_{\mathbf{k}} = \hat{\mathbf{\Theta}}_{\mathbf{k}} \mathbf{\Lambda}_{\mathbf{k}} \hat{\mathbf{\Theta}}_{\mathbf{k}}^H, \quad (5)$$

and the SPOD modes are obtained from $\hat{\mathbf{\Theta}}_{\mathbf{k}}$ as,

$$\mathbf{\Psi}_{\mathbf{k}} = \hat{\mathbf{Y}}_{\mathbf{k}} \hat{\mathbf{\Theta}}_{\mathbf{k}} \mathbf{\Lambda}_{\mathbf{k}}^{-1/2}, \quad (6)$$

where $\hat{\mathbf{Y}}_{\mathbf{k}} \triangleq [\hat{\mathbf{y}}_{\mathbf{k}(1)} \hat{\mathbf{y}}_{\mathbf{k}(2)} \cdots \hat{\mathbf{y}}_{\mathbf{k}(P)}]$ denotes the ensemble matrix for different realisations of $\hat{\mathbf{y}}_{\mathbf{k}}$ with P being the total number of realisations, $\mathbf{\Psi}_{\mathbf{k}}$ and $\mathbf{\Lambda}_{\mathbf{k}}$ are SPOD modes and their associated eigenvalues, respectively (see Towne *et al.* (2018)), and \mathbf{W} is a positive-definite matrix of quadrature gains along y , which is discretised.

In Karban *et al.* (2022), it is shown that this coefficient matrix $\hat{\mathbf{\Theta}}_{\mathbf{k}}$ can be used to extract the part in the forcing that is correlated with the observed SPOD mode as,

$$\boldsymbol{\chi}_{\mathbf{k}} = \hat{\mathbf{F}}_{\mathbf{k}} \hat{\mathbf{\Theta}}_{\mathbf{k}} \mathbf{\Lambda}_{\mathbf{k}}^{-1/2}, \quad (7)$$

where, $\hat{\mathbf{F}}_{\mathbf{k}}$ is the ensemble matrix of $\hat{\mathbf{f}}_{\mathbf{k}}$. The RESPOD forcing mode $\boldsymbol{\chi}_{\mathbf{k}}$ satisfies,

$$\mathbf{\Psi}_{\mathbf{k}} = \mathbf{R}_{\mathbf{k}} \boldsymbol{\chi}_{\mathbf{k}}. \quad (8)$$

Given the expansion in (4), $\boldsymbol{\chi}_{\mathbf{k}}$ can be decomposed as,

$$\boldsymbol{\chi}_{\mathbf{k}} = \sum_{\mathbf{i}} \Gamma_{\mathbf{i}, \mathbf{k}-\mathbf{i}} \triangleq \sum_{\mathbf{i}} \hat{\mathbf{U}}_{\mathbf{i}} \nabla \hat{\mathbf{U}}_{\mathbf{k}-\mathbf{i}} \hat{\mathbf{\Theta}}_{\mathbf{k}} \mathbf{\Lambda}_{\mathbf{k}}^{-1/2}, \quad (9)$$

where $\hat{\mathbf{U}}$ denotes the ensemble matrix of $\hat{\mathbf{u}}$. We define the over-all energy of a flow structure, $\boldsymbol{\xi}$, as,

$$\|\boldsymbol{\xi}\|^2 = \varepsilon\{\boldsymbol{\xi}^H \mathbf{W} \boldsymbol{\xi}\}, \quad (10)$$

where the superscript H indicates Hermitian transpose, and $\varepsilon\{\cdot\}$ denotes the expectation operator. In what follows, $\varepsilon\{\cdot\}$ corresponds to time-averaging for time-dependent structures, and to ensemble averaging for Fourier realisations in frequency space. The energy of $\Gamma_{\mathbf{i}, \mathbf{k}-\mathbf{i}}$, denoted by $\|\Gamma_{\mathbf{i}, \mathbf{k}-\mathbf{i}}\|^2$, for all \mathbf{i} shows the correlation map of the nonlinear interactions related to the observed SPOD mode, $\mathbf{\Psi}_{\mathbf{k}}$. This includes the ‘silent’ correlations (Karbon *et al.*, 2022). One can exclude the effect of the silent-but-correlated part by investigating $\|\mathbf{R}_{\mathbf{k}} \Gamma_{\mathbf{i}, \mathbf{k}-\mathbf{i}}\|^2$. Equation (8) implies that such a map indicates the contribution of different nonlinear interactions to a given SPOD mode of the measured state.

3 DETAILS OF THE DNS OF THE COUETTE FLOW

The use of RESPOD for detection of ‘important’ non-linear interactions associated with a specific measurement is tested on a minimal Couette flow, similar to that investigated in Nogueira *et al.* (2021). The simulations are performed using ‘ChannelFlow’ code, a pseudo-spectral incompressible flow solver using a Fourier-Chebyshev discretisation in the wall-parallel and wall-normal directions, respectively (see www.channelflow.ch for details). The dimensions of the minimal box are $(L_x, L_y, L_z) = (1.75\pi h, 2h, 1.2\pi h)$, where the subscripts x , y and z denote the streamwise, wall-normal and spanwise directions, and h is the channel half-height. The domain was discretised as $(n_x, n_y, n_z) = (32, 65, 32)$ with a dealiasing factor of 3/2 in the wall-parallel directions. The channel walls move with wall velocity, $\pm U_w$ yielding a Reynolds number, $Re = 400$ based on U_w and h , which corresponds to a friction Reynolds number, $Re_\tau \approx 34$. The flow data was stored, once the initial transients disappeared, for 300 convective units with a sampling rate, $\Delta t = 0.1$. Temporal data is transformed into frequency space using blocks of 1024 time steps with 50% overlapping and using the exponential windowing function given in Martini *et al.* (2019) with $n = 2$.

Figure 1 presents the profiles for the mean and the root-mean-square (RMS) of the velocity components, u , v and w in the streamwise, wall-normal and spanwise directions, respectively, along the wall-normal direction, y . We see that the mean flow is deviated from the laminar solution given by $-(y-1)$ due to nonlinear interactions between turbulent fluctuations. The RMS plots indicate that the fluctuations in u peak around $y = 1.5$ and $y = 0.5$. A similar but smaller double-peak structure is seen in the RMS of w with the peaks occurring at the same wall-normal positions. The RMS of v peaks around the center at an amplitude slightly less than that of w .

We choose wall shear fluctuations in the spanwise direction, $\tau_z \triangleq \partial_z u'|_{y=\{-1,1\}}$ at both upper and lower walls as our observable. Spanwise wall shear was used to extract self-similar wall-attached structures in a turbulent channel in Karban *et al.* (2022). Here, we use it simply to have a low-rank representation of the flow, associated with this quantity.

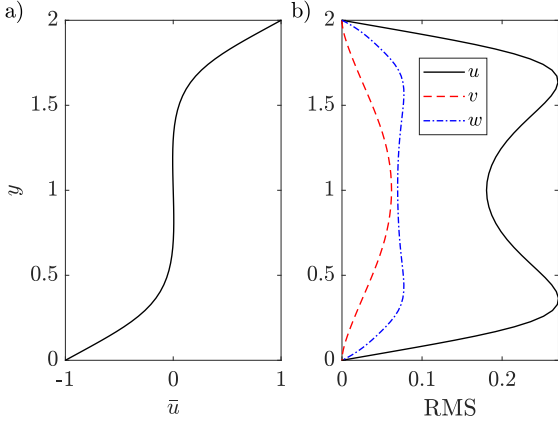


Figure 1. Mean (a) and the RMS (b) profiles of the velocity components, u (black solid), v (red dashed) and w (blue dash-dotted) along the wall-normal direction.

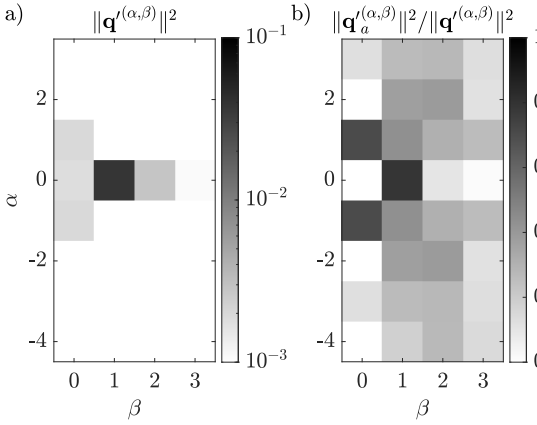


Figure 2. a) Energy of flow structures at different wavenumber pairs averaged over time. b) Ratio of the average energy of the wall-attached structures to that of the wall-attached and detached structures added together.

For simpler notation, wavenumbers will be presented in integers defined as $\alpha = \tilde{\alpha}L_x/2\pi$ and $\beta = \tilde{\beta}L_z/2\pi$. Similarly, mode frequencies will be presented in integer bins denoted by $\omega = \tilde{\omega}N_F/f_s$, ranging in $[-N_F/2, N_F/2 - 1]$, where $N_F = 1024$ is the number of temporal points used for taking the Fourier transform (FT) and $f_s \triangleq 1/\Delta t$ is the sampling rate of the database.

Figure 2 shows the time-averaged energy contained in each wavenumber pair together with the ratio of the time-averaged energy of the wall-attached structures to the entire turbulent fluctuations at each wavenumber pair. We see that the mode pair $(\alpha, \beta) = (0, 1)$, related to streaks and rolls spanning the entire computational domain, contains the most of the fluctuation energy ($\sim 75\%$) while the modes $(\pm 1, 0)$ and $(0, 2)$ contains slightly less than 5% of the total energy and all the other mode pairs contain less than 2%. The energy of the wall-attached part of the state, denoted by \mathbf{q}_a , of the mode $(0, 1)$ is around 80% of its total energy. Therefore, the coherent structures correlated with the spanwise wall-shear can be said to constitute a good low-rank representative of the flow at this wavenumber pair. A similar case is observed for the modes $(0, \pm 1)$ while for the mode $(0, 2)$, the energy ratio of the wall-attached part is around 15%.

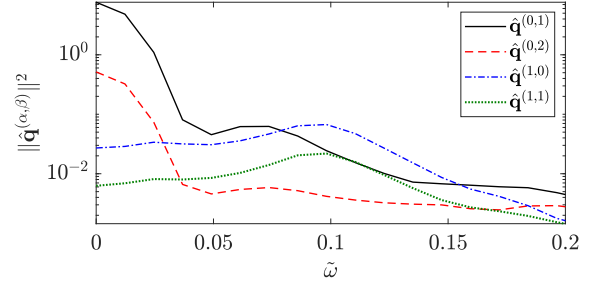


Figure 3. PSDs of $\hat{\mathbf{q}}^{(0,1)}$ (blue), $\hat{\mathbf{q}}^{(0,2)}$ (orange), $\hat{\mathbf{q}}^{(1,0)}$ (yellow) and $\hat{\mathbf{q}}^{(1,1)}$ (violet) integrated over the wall-normal direction.

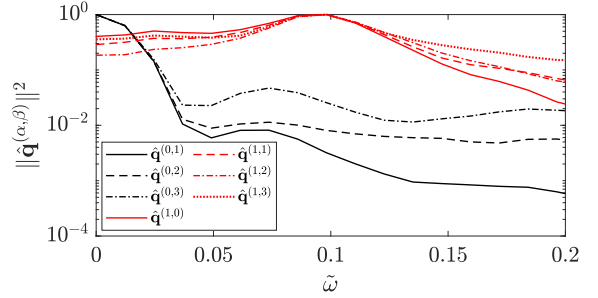


Figure 4. PSDs of $\hat{\mathbf{q}}^{(0,\{1,3\})}$ (black; solid, dashed, dash-dotted, respectively), and $\hat{\mathbf{q}}^{(1,\{0,3\})}$ (red; solid, dashed, dash-dotted, dotted, respectively) integrated over the wall-normal direction and normalised with respect to the peak value of each mode.

Figure 3 shows the power spectral densities (PSD) integrated along the wall-normal direction for the modes $(\alpha, \beta) = (0, 1)$, $(0, 2)$, $(1, 0)$ and $(1, 1)$. Although the mode $(\alpha, \beta) = (1, 1)$ is energy-wise insignificant, it plays a critical role for transfer of energy to $(\alpha, \beta) = (0, 1)$ mode, as will be shown later, and hence is included here. We see that the streamwise-constant modes peak around the zero frequency while the $(1, 0)$ and $(1, 1)$ modes have their peak around $\tilde{\omega} \approx 0.1$ ($\omega = 8$). The shape of the spectra is observed to be similar for the modes that have the same streamwise wavenumber. This trend can be more clearly seen in figure 4, where the integrated PSDs normalised with respect to the peak value are plotted for different modes. We see two different families of PSD distributions for the two streamwise wavenumbers, $\alpha = 0$ and $\alpha = 1$, respectively.

We now focus on the most energetic mode $(\alpha, \beta) = (0, 1)$ at its peak-energy frequency, $\omega = 0$. The wall-attached response and forcing modes are shown in figure 5. The response field consists of streaks and streamwise vortices. Given that the upper and lower walls have positive and negative velocities, respectively, the phase relation between streaks and the streamwise vortices is reminiscent of lift-up mechanism (Brandt, 2014). This is further supported regarding the associated forcing mode. At the spanwise positions where the streamwise vortices are located, the forcing is mainly located near the walls aligned with the y -direction, causing a moment to generate the streamwise vortices. These vortices then generate streaks by carrying the high- and low-velocity structure near the upper and lower walls, respectively, towards the channel center. Note that the forcing component in the streamwise direction is indeed in opposite phase to the streaks seen in

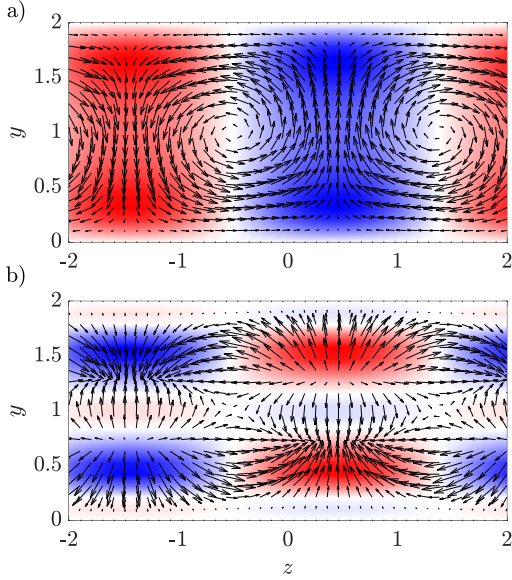


Figure 5. Wall-attached part of the velocity (a) and the associated forcing (b) reconstructed in the y - z plane for the mode $(\alpha, \beta, \omega) = (0, 1, 0)$. The color plot indicates the streamwise component and the arrows show the spanwise and wall-normal components.

the response. This indicates that the streaks are generated by the lift-up mechanism despite the counteracting effect of the streamwise forcing, as previously reported by Nogueira *et al.* (2021). The response generation at this triplet can therefore be considered suboptimal.

4 NONLINEAR INTERACTIONS IN THE MINIMAL COUETTE FLOW

4.1 Extracting important triadic interactions

The interaction maps obtained by computing via (10) the energy associated with a nonlinear interaction contributing to the target mode, $\mathbf{k} = (\alpha_k, \beta_k, \omega_k) = (0, 1, 0)$ are shown in figure 6. Different columns compares the maps $\|\hat{\mathbf{u}}_i \nabla \hat{\mathbf{u}}_{\mathbf{k}-\mathbf{i}}\|^2$, $\|\mathbf{\Gamma}_{\mathbf{i}, \mathbf{k}-\mathbf{i}}\|^2$ and $\|\mathbf{R}_k \mathbf{\Gamma}_{\mathbf{i}, \mathbf{k}-\mathbf{i}}\|^2$, which correspond to the direct triadic interactions, the wall-correlated triadic interactions, and the wall-correlated triadic interactions filtered by the resolvent operator, respectively. Note that only the triplet $\mathbf{i} = (\alpha_i, \beta_i, \omega_i)$ is shown, where for each \mathbf{i} , there exists a $\mathbf{k} - \mathbf{i}$ yielding $\mathbf{k} = (0, 1, 0)$. We see that the interaction between $(0, -1, 0)$ and its complementary, $(0, 2, 0)$, is dominant in all three maps, indicating that the interaction is large in amplitude, highly correlated to the target mode, and generates the response with the largest amplitude. We also observe large amplitude for the interaction $(0, 2, 0) + (0, -1, 0)$, which involves the same structures with the previous one, but with the gradient operator acting on the $(0, -1, 0)$ mode. The interactions $(\pm 1, 1, 0) + (\mp 1, 0, 0)$, although not yielding a large forcing component, are seen to be present in the response map, implying the efficiency of these modes in driving the observable.

To investigate the overall contribution to the target mode $(0, 1, 0)$ via all the triadic interactions associated with a given wavenumber pair (α_i, β_i) , we define the forcing mode, $\check{\mathbf{\Gamma}}_{\mathbf{i}, \mathbf{k}-\mathbf{i}}$ obtained by integrating $\mathbf{\Gamma}_{\mathbf{i}, \mathbf{k}-\mathbf{i}}$ over the frequency index, ω_i , and compute its response via $\mathbf{R}_k \check{\mathbf{\Gamma}}_{\mathbf{i}, \mathbf{k}-\mathbf{i}}$. The interaction map $\|\mathbf{R}_k \check{\mathbf{\Gamma}}_{\mathbf{i}, \mathbf{k}-\mathbf{i}}\|^2$ is plotted in figure 7, which shows that the response generation is dominated by six interac-

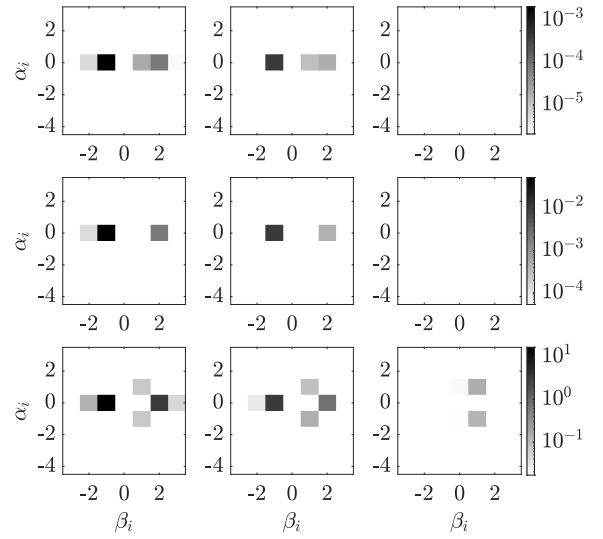


Figure 6. Amplitude maps of $\|\hat{\mathbf{u}}_i \nabla \hat{\mathbf{u}}_{\mathbf{k}-\mathbf{i}}\|^2$ (top), $\|\mathbf{\Gamma}_{\mathbf{i}, \mathbf{k}-\mathbf{i}}\|^2$ (middle), and $\|\mathbf{R}_k \mathbf{\Gamma}_{\mathbf{i}, \mathbf{k}-\mathbf{i}}\|^2$ (bottom) obtained at $\omega_i = 0$ (left), $\omega_i = 4$ (center) and $\omega_i = 8$ (right), for the target mode $\mathbf{k} = (\alpha_k, \beta_k, \omega_k) = (0, 1, 0)$. Only the modes \mathbf{i} are shown while the complementary modes $\mathbf{k} - \mathbf{i}$ are selected to yield $\mathbf{k} = (0, 1, 0)$.

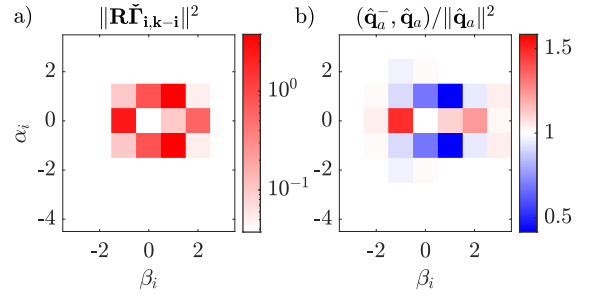


Figure 7. a) Amplitude map of the response generated by the wall-correlated interactions at all frequencies added together. b) The map of normalised inner product between the overall response and the response with contribution of a single interaction masked, computed at different wavenumber pairs used for masking. The target mode for both maps is $(\alpha_k, \beta_k, \omega_k) = (0, 1, 0)$.

tions: two streamwise-constant, which are $(0, \{-1, 2\}) + (0, \{2, -1\})$, and four streamwise-periodic over L_x , which are $(\pm 1, \{0, 1\}) + (\mp 1, \{1, 0\})$. Note that here and in what follows, we use curly brackets for short hand notation of multiple modes. For instance, $(0, \{-1, 2\})$ denotes the modes $(0, -1)$ and $(0, 2)$.

To understand whether a given interaction has a destructive or constructive effect on the response, instead of computing its individual response, we calculate the overall response with that particular interaction masked, i.e., its contribution is not included in the response. We denote this masked wall-attached response as $\hat{\mathbf{q}}_a^-$ and investigate the change in the response energy due to this masking by computing the inner product,

$$(\hat{\mathbf{q}}_a^-, \hat{\mathbf{q}}_a) \triangleq \varepsilon \{ \hat{\mathbf{q}}_a^{-H} \mathbf{W} \hat{\mathbf{q}}_a \}. \quad (11)$$

An interaction map is obtained obtained by calculating (11)

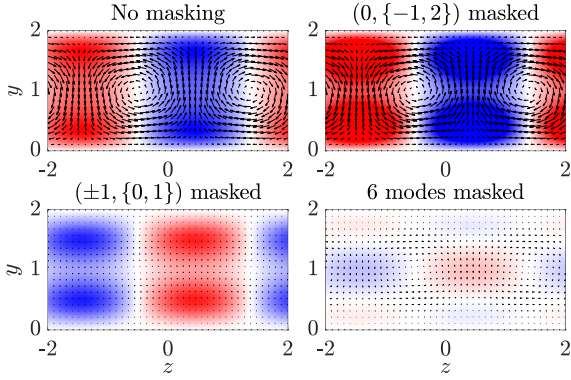


Figure 8. Velocity field corresponding to the wall-attached structure $(\alpha_k, \beta_k, \omega_k) = (0, 1, 0)$ in the y - z plane. Top-left: the entire response; top-right: the response obtained by masking the interactions between the modes $(\alpha_i, \beta_i) = (0, \{-1, 2\})$ and their complementary modes; bottom-left: the response obtained by masking the interactions between the modes $(\alpha_i, \beta_i) = (\pm 1, \{0, 1\})$ and their complementary modes; bottom-right: the response obtained by masking the interactions between the modes $(\alpha_i, \beta_i) = (0, \{-1, 2\})$ and their complementary modes as well as the interactions between the modes $(\alpha_i, \beta_i) = (\pm 1, \{0, 1\})$ and their complementary modes.

by individually masking each wavenumber pair and normalising the result with $\|\hat{q}_\alpha\|^2$ as shown in figure 7-b. The analysis reveals that masking the contributions from the interactions $(0, \{-1, 2\}) + (0, \{2, -1\})$ increases the response energy, implying a destructive interference between these interactions and the remaining ones. Masking the contributions from the interactions $(\pm 1, \{0, 1\}) + (\mp 1, \{1, 0\})$, on the other hand, causes the response energy to decrease, implying that these interactions have a constructive effect on the response.

The effect of these masking operations on the response field is shown in figure 8. We see that masking the interactions $(0, \{-1, 2\}) + (0, \{2, -1\})$ mainly affects the streaks causing an increase in their amplitude, while the streamwise vortex remains nearly unchanged. Masking the interactions $(\pm 1, \{0, 1\}) + (\mp 1, \{1, 0\})$, almost completely eliminates the streamwise vortices, which also causes the lift-up effect to be eliminated. This results in streaks with smaller amplitude and reversed phase. This result is consistent with the idea of a self-sustaining process in wall turbulence, with streamwise vortices excited by non-linear interactions involving waves with non-zero α (Hamilton *et al.*, 1995; Hall & Sherwin, 2010). Remember that in the RESPOD forcing mode shown in figure 5, the streamwise component counteracts the lift-up mechanism forced by the spanwise components. These results, when combined, imply that the streamwise and spanwise components in the RESPOD forcing mode, χ_k , are mainly constructed by the nonlinear interaction groups $(0, \{-1, 2\}) + (0, \{2, -1\})$ and $(\pm 1, \{0, 1\}) + (\mp 1, \{1, 0\})$, respectively. Masking $(\pm 1, \{0, 1\}) + (\mp 1, \{1, 0\})$ causes the lift-up mechanism, which is an efficient means to generate streaks via streamwise vortices, to disappear. The remaining streamwise component in χ_k is mainly constructed by $(0, \{-1, 2\}) + (0, \{2, -1\})$ and generates streaks with negative phase, reducing the amplitude of the streaks generated by the lift-up mechanism. Masking all six modes eliminates almost entirely the response as seen in figure 8.

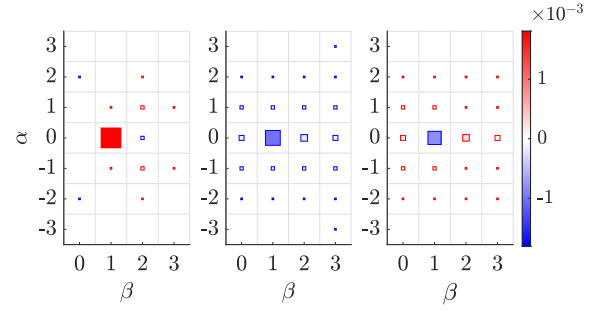


Figure 9. Production (left), dissipation (center), and nonlinear transfer (right) of the spectral turbulent kinetic energy for different wavenumber pairs. Both the size and the color intensity of the markers indicate amplitude.

4.2 Energy transfer via triadic interactions

The interaction map shown in figure 7-b can also be interpreted in terms of energy exchange between different modes via nonlinear interactions. Symon *et al.* (2021) investigated, by employing the spectral form of the transport equation of turbulent kinetic energy (TKE), the overall relation between production, dissipation and the transfer of energy for individual wavenumber pairs in parallel stationary turbulent flows. The spectral TKE equation is given in indicial notation as,

$$\frac{\partial \hat{E}}{\partial t} = - \int_0^2 \frac{\partial \bar{u}}{\partial y} \bar{u}^* \hat{v} dy - \frac{1}{Re} \int_0^2 \frac{\partial \hat{u}_m}{\partial x_n} \frac{\partial \hat{u}_m^*}{\partial x_n} dy - \int_0^2 \hat{u}_m^* \hat{f}_m dy, \quad (12)$$

where the hat in this equation denotes, by abuse of notation, Fourier transformed quantities in the streamwise and spanwise directions, \hat{E} is the spectral TKE, the superscript * denotes complex conjugate, m and n denote that the vector indices, \hat{f}_m is the m^{th} component of the forcing vector (see Symon *et al.* (2021) for derivation of (12)). Here, we assume that the Couette flow is stationary in the time interval we investigate, which renders

$$\frac{\partial \hat{E}}{\partial t} = 0. \quad (13)$$

The three terms on the right hand side of (12) correspond to the production, dissipation and nonlinear transfer of the turbulent kinetic energy, which, thanks to (13), sum up to zero for a given wavenumber pair. The contributions of production, dissipation and nonlinear transfer to the energy balance for different wavenumber pairs are illustrated in figure 9. We see that the $(0, 1)$ mode draws the most energy from the mean flow to produce TKE, and is the only mode to transfer this energy to other modes via nonlinear transfer. All the modes are seen to lose energy via dissipation as expected.

The analysis done by computing (11), as a complementary tool to the energy balance analysis discussed above, provides information about the transfer of energy between individual modes. A red square in the interaction map shown in figure 7-b implies that the target mode is losing energy via the associated nonlinear interaction, while a blue spot indicates the opposite. One can investigate interaction maps for different target modes to understand the paths of energy transfer among different modes. In figure 10, we show the same interaction map given in figure 7-b for the target modes

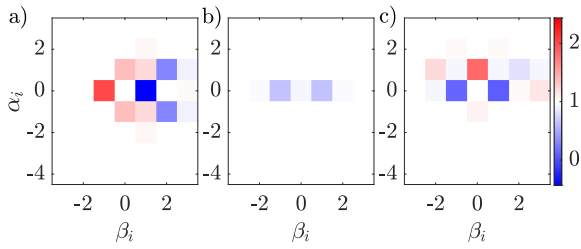


Figure 10. The same map with figure 7-b obtained for the target modes $(\alpha_k, \beta_k, \omega_k) = (0, 2, 0)$ (a), $(1, 0, 8)$ (b) and $(1, 1, 8)$ (c).

$(\alpha_k, \beta_k, \omega_k) = (0, 2, 0)$, $(1, 0, 8)$ and $(1, 1, 8)$. Note that the frequency index for each target mode is selected as the peak-energy containing frequency for the interaction maps to be a better representative of the energy transfer in the corresponding wavenumber pair. We seen in figure 10 that all three target modes receive energy from the interactions involving the $(0, 1)$ mode. This is expected since the $(0, 1)$ mode receives the largest energy from the mean flow, similar to the cases shown in Symon *et al.* (2021), and distributes them into other modes via nonlinear transfer. Comparing figures 7-b and 10-a reveals that the energy transfer between the modes $(0, 1)$ and $(0, 2)$ is one way, going from $(0, 1)$ to $(0, 2)$, which, when blocked, increases the energy in the mode $(0, 1)$ and decreases that in $(0, 2)$. The energy transfer between $(0, 1)$ and $(1, 1)$, on the other hand, is two way, i.e., the two modes transfer energy to each other via different triadic interactions. A similar relation exists between $(0, 1)$ and $(1, 0)$.

5 CONCLUSIONS

We have discussed a method to investigate the triadic interactions that underpin the generation of flow structures associated with a given observable. The method is based on the resolvent-based extended spectral proper orthogonal decomposition (RESPOD), used in Karban *et al.* (2022) to identify self-similar structures in a turbulent channel flow. A minimal Couette flow is here chosen as the test case, where the triadic interactions associated with spanwise wall-shear are investigated.

The analysis reveals that the most energetic mode, $(\alpha, \beta) = 0$, at its peak-energy frequency, $\omega = 0$, was mainly driven by six triadic interactions: four interactions involving modes periodic over L_x in the streamwise direction, that generate small-in-amplitude but efficient forcing, and two interactions involving streamwise-constant modes that generate forcing structures large in amplitude, and thus effective in driving the observable. The streamwise-periodic interactions generate a combined streak-streamwise vortex structure via the lift-up mechanism, while the streamwise-constant interactions counteract the streak generation by generating a streamwise forcing component in phase opposition to the lift-up mechanism. This explains in physical terms the destructive interference of forcing observed by Nogueira *et al.* (2021) forcing comprises different triadic interactions, with opposing effects in exciting streamwise vortices and streaks.

Our framework also allows us to investigate energy transfer between different modes via triadic interactions. We observe that the triadic interactions involving the $(0, 1)$ mode provides a constructive contribution to all the modes we investigated. This is an expected result since it is the only mode with negative nonlinear transfer rate of turbulent kinetic energy as

shown by the energy balance analysis we conducted following Symon *et al.* (2021). The relation between $(0, 1)$ and the streamwise-constant modes $(0, \{-1, 2\})$ is shown to be a one-way energy transfer which causes the $(0, 1)$ mode to lose its energy. The relation between $(0, 1)$ and the streamwise periodic modes $(\pm 1, 0, 1)$, on the other hand, is found to be in two ways, with energy transfers in both directions.

The method we discuss provides a systematic means by which to understand mechanisms active in the generation of a given observable in a turbulent flow, which can be freely determined via a measurement matrix, thanks to the flexibility of the resolvent framework. This makes application of this approach to more complicated flows possible.

REFERENCES

- Bae, H. Jane, Lozano-Durán, A. & McKeon, Beverley J. 2021 Nonlinear mechanism of the self-sustaining process in the buffer and logarithmic layer of wall-bounded flows. *Journal of Fluid Mechanics* **914**, A3.
- Borée, J 2003 Extended proper orthogonal decomposition: a tool to analyse correlated events in turbulent flows. *Experiments in fluids* **35** (2), 188–192.
- Brandt, Luca 2014 The lift-up effect: The linear mechanism behind transition and turbulence in shear flows. *European Journal of Mechanics, B/Fluids* **47**, 80–96.
- Hall, Philip & Sherwin, Spencer 2010 Streamwise vortices in shear flows: harbingers of transition and the skeleton of coherent structures. *Journal of Fluid Mechanics* **661**, 178–205.
- Hamilton, James M., Kim, John & Waleffe, Fabian 1995 Regeneration mechanisms of near-wall turbulence structures. *Journal of Fluid Mechanics* **287**, 317–348.
- Hoarau, C., Borée, J., Laumonier, J. & Gervais, Y. 2006 Analysis of the wall pressure trace downstream of a separated region using extended proper orthogonal decomposition. *Physics of Fluids* **18**, 055107.
- Karban, U., Martini, E., Cavalieri, A.V.G., Lesshafft, L. & Jordan, P. 2022 Self-similar mechanisms in wall turbulence studied using resolvent analysis. *Journal of Fluid Mechanics* **939**, A36.
- Martini, E., Cavalieri, A. V., Jordan, P. & Lesshafft, L. 2019 Accurate frequency domain identification of odes with arbitrary signals. *arXiv: Signal Processing*.
- McKeon, B. J. & Sharma, A. S. 2010 A critical-layer framework for turbulent pipe flow. *Journal of Fluid Mechanics* **658**, 336–382.
- Nogueira, Petrônio A. S., Morra, Pierluigi, Martini, Eduardo, Cavalieri, André V. G. & Henningson, Dan S. 2021 Forcing statistics in resolvent analysis: application in minimal turbulent couette flow. *Journal of Fluid Mechanics* **908**, A32.
- Symon, Sean, Illingworth, Simon J. & Marusic, Ivan 2021 Energy transfer in turbulent channel flows and implications for resolvent modelling. *Journal of Fluid Mechanics* **911**.
- Towne, Aaron, Colonius, Tim, Jordan, Peter, Cavalieri, André V. & Brès, Guillaume A. 2015 *Stochastic and nonlinear forcing of wavepackets in a Mach 0.9 jet*.
- Towne, Aaron, Schmidt, Oliver T. & Colonius, Tim 2018 Spectral proper orthogonal decomposition and its relationship to dynamic mode decomposition and resolvent analysis. *Journal of Fluid Mechanics* **847**, 821–867.